Nanoscale

PAPER

View Article Online
View Journal | View Issue

Cite this: *Nanoscale*, 2022, **14**, 8041

TiO_2-Modulated tetra(4-carboxyphenyl)porphyrin/perylene diimide organic Z-scheme nano-heterojunctions for efficient visible-light catalytic CO_2 reduction†

Yilin Wang,[a] Zhenlong Zhao,[a] Rui Sun,[b] Ji Bian, *[a] Ziqing Zhang*[a] and Liqiang Jing *[a,b]

Developing efficient Z-scheme heterojunctions with wide visible-light responsive perylene diimide (PDI) is highly desired for CO_2 conversion, while the effective charge transfer and separation are crucial. Herein, TiO_2-modulated tetra(4-carboxyphenyl)porphyrin/perylene diimide (T-TP/PDI) organic nano-heterojunctions have been fabricated for CO_2 reduction, in which TP and PDI are first assembled *via* π–π interactions between their similar 2D conjugate structures, and then the TiO_2 nanoparticles (*ca.* 10 nm) are anchored as an energy platform through the carboxyl groups on TP. The optimal one exhibits a ~10-fold enhancement in photocatalytic activity compared with the pristine PDI. Based on the time-resolved surface photovoltage responses, electron paramagnetic resonance signals, *in situ* diffuse reflectance infrared Fourier transform spectra and the amount evaluation of H_2O_2 as the water-oxidation intermediate, it is suggested that the exceptional photoactivity be ascribed to the accelerated charge transfer and separation resulting from the constructed Z-scheme nano-heterojunctions with intimate interfacial interactions and the introduced energy platform TiO_2 oriented towards largely inhibiting the type-II charge transfer pathway. This work diversifies the strategies for constructing efficient organic Z-scheme heterojunctions, and provides insight into interface correlation among components.

Received 30th March 2022,
Accepted 13th May 2022

DOI: 10.1039/d2nr01753a

rsc.li/nanoscale

Introduction

The consumption of fossil fuels and excessive CO_2 emissions have led to serious energy and environmental crises.[1–3] Photocatalytic CO_2 reduction is one of the most promising approaches to mitigate these crises by utilizing renewable solar energy to convert CO_2 into high value-added carbonaceous fuels.[4,5] Enormous efforts have been dedicated to develop efficient semiconductor photocatalysts for CO_2 reduction.[6] Typical inorganic semiconductor photocatalysts (*e.g.*, TiO_2,[7] Bi_2MoO_6,[8] BiOX,[9] *etc.*) have been widely investigated and proven to be efficient for CO_2 reduction; however, there still remain several intrinsic drawbacks limiting their photocatalytic activities, including limited visible-light harvesting, difficulties in tuning the structures and high costs of raw materials. In contrast, organic materials have enormous advantages in tunable optical and electronic properties, structural diversity and Earth-abundance.

Perylene-3,4,9,10-tetracarboxylic diimide (PDI), an emerging class of n-type organic semiconductors, has been intensively explored in applications of photocatalysis, fluorescent sensors, light emitting diodes, *etc.* by virtue of its unique optical and electronic properties, electron affinity and charge carrier mobility.[10–15] Unfortunately, the intrinsic insolubility of commercially available PDI makes it difficult to tailor surface properties through the self-assembly process, seriously limiting its photocatalytic activity.[16] Zhu *et al.* report a self-assembly method of rapid solution dispersion to obtain a non-covalent PDI supramolecular system, which exhibited remarkable visible-light catalytic properties for degradation of phenol and splitting water for O_2 evolution.[17] This method provides a feasible route for fabricating a self-assembled PDI supramolecular system with a two-dimensional (2D) structure.

Although the wide visible-light responsive PDI supramolecular system exhibits excellent photocatalytic oxygen evolution, it is still unsatisfactory to be a candidate for photocatalytic

[a]*Key Laboratory of Functional Inorganic Materials Chemistry (Ministry of Education), School of Chemistry and Materials Science, International Joint Research Center for Catalytic Technology, Heilongjiang University, Harbin 150080, P. R. China. E-mail: bianji@hlju.edu.cn, zhangzq@hlju.edu.cn, jinglq@hlju.edu.cn*
[b]*Key Lab of Groundwater Resources and Environment of Ministry of Education, Key Lab of Water Resources and Aquatic Environment of Jilin Province, College of New Energy and Environment, Jilin University, Changchun 130012, P. R. China*
† Electronic supplementary information (ESI) available. See DOI: https://doi.org/10.1039/d2nr01753a

CO_2 reduction due to its positive conduction band (CB) and sluggish charge separation.[10] As inspired by natural photosynthesis, a Z-scheme heterojunction hosting a reduction photocatalyst (RP) and an oxidation photocatalyst (OP) is capable of not only enhancing the charge separation, but also maintaining the superior redox capacity of the RP and OP.[18,19] Typically, inorganic photocatalysts with positive valence bands (VBs), such as $BiVO_4$,[20] WO_3,[21] Fe_2O_3,[22] *etc.*, are investigated as OPs, which could offer sufficient thermodynamic driving force for oxidation half-reaction. Considering the superior oxidation capacity and wide visible-light responsive nature of PDI,[23] it should be greatly advantageous to construct a Z-scheme heterojunction with a PDI supramolecular system by substituting inorganic metal oxides as OPs. Thus, it is significant to choose a properly matched RP to couple with PDI. Typical g-C_3N_4,[24,25] sulfides[26,27] *etc*. with negatively positioned CBs are benign candidates that could be used as RPs, whereas their limited visible-light absorption and inferior photostability still severely hamper their applications to some extent. In contrast, porphyrin molecules containing the porphyrin ring and diverse substituents (carboxyl, hydroxyl or sulfonic acid groups) capture our interest due to their wide absorption spectrum even to the entire natural spectrum.[28] Fortunately, the highest occupied molecular orbital (HOMO) energy levels of porphyrin molecules are close to the CB of PDI, and their similar conjugated macrocycle structures are favorable to build a dimension-matched interface through π–π interactions, inspiring us to select porphyrins as RPs to construct a full-spectrum responsive Z-scheme heterojunction with PDI.[29]

Indeed, the core of an efficient Z-scheme heterojunction is the rapid photogenerated charge transfer and separation for the long-lived charge carriers, especially for the organic Z-scheme heterojunction system.[30] In our previous work, incorporation of a wide bandgap semiconductor on a RP as the energy platform has been demonstrated as a universal strategy for constructing a cascade Z-scheme system by extracting the energetic electrons accumulated on the CB of RP, so as to direct Z-scheme charge transfer and separation and block the unexpected type-II charge transfer pathway effectively.[31] Accordingly, it is predictable that introducing an energy platform like TiO_2 on RP porphyrin molecules is bound to strengthen the Z-scheme charge transfer and hence prolong the lifetimes of separated photoelectrons. In general, the robust interface connection between porphyrin and TiO_2 is quite crucial. As the surfaces of nanosized TiO_2 generally have abundant hydroxyl groups,[32] it provides a feasible path to form efficient connection with porphyrin molecules through its substituents. Tetra(4-carboxylphenyl)porphyrin (TCPP), one of the porphyrin molecules containing carboxylic groups, possesses excellent photostability and could be combined strongly onto metal oxides.[33,34] Thus, it is expected to simultaneously achieve closely connected 2D/2D interfaces with PDI by π–π interactions from its porphyrin ring and effective introduction of an energy platform with its carboxylic groups. Obviously, TiO_2 modified TCPP/PDI Z-scheme nano-heterojunction systems are extremely desired for exceptional solar-driven CO_2 conversion, which has been rarely reported up to now.

Herein, elaborated TiO_2-modulated TCPP/PDI organic Z-scheme nano-heterojunctions (T-TP/PDI) have been fabricated for CO_2 reduction, where TP and PDI are first assembled *via* π–π interactions, and then TiO_2 nanoparticles (*ca.* 10 nm) are anchored through the carboxyl groups on TP. The optimal 5T-10TP/PDI exhibits an ~10-fold enhancement in photocatalytic activity compared with the pristine PDI, which is mainly ascribed to the intimate interfacial interactions and the promoted Z-scheme charge transfer. The cascade Z-scheme charge transfer mechanism with an introduced energy platform is well confirmed, and the effect of carboxyl groups in TP is revealed in detail.

Experimental

Synthesis of ultrathin PDI nanosheets

In a typical experiment, 100 mg of commercial perylene-3,4,9,10-tetracarboxylic diimide was dissolved in 10 mL of concentrated sulfuric acid (H_2SO_4) to form a purplish red solution. After ultrasonic treatment for 2 h, 100 mL of H_2O was added into the above solution in an ice bath and kept for 30 min to obtain a suspension with dark purple solids. Afterwards, the dark purple solids were obtained by centrifugation, then washed to neutrality with H_2O and dried at 60 °C in an oven. The obtained self-assembled ultrathin PDI nanosheets were denoted as PDI.

Synthesis of TCPP coupled PDI heterojunctions (TP/PDI)

A series of TP/PDI heterojunctions were obtained by a wet chemical approach. First, 0.1 g of PDI and a certain amount of commercial TCPP were dispersed in 50 mL of ethanol solution. The above suspension was stirred and sonicated for 30 min in turn, and the procedure was repeated three times. Then the mixture was dried at 80 °C in a water bath to completely evaporate ethanol. Finally, the catalyst was dried under vacuum at 80 °C overnight. The samples were denoted as *x*TP/PDI (x = 5, 10 and 15, representing the mass ratio percentage of TP to PDI).

Synthesis of TiO_2 coupled TP/PDI heterojunctions (T-TP/PDI)

First, a 10TP/PDI heterojunction was synthesized in accordance with the above method, and then TiO_2 was incorporated on it as follows. The desired amounts of TiO_2 and 10TP/PDI were dispersed in 100 mL of ethanol, followed by ultrasonication for 30 min. Then the mixture was refluxed at 80 °C for 3 h. Finally, the obtained sample was washed with deionized water 4 times, and dried under vacuum at 80 °C overnight. The samples were denoted as *y*T-10TP/PDI (y = 3, 5, and 7, determined by the mass ratio percentage of TiO_2 to PDI).

Photocatalytic activities for CO_2 conversion

The photocatalytic reaction was conducted in a gas–solid reaction system. In detail, the photocatalyst (20 mg) was dispersed at the bottom of a quartz cell reactor (100 mL) equipped with a 300 W xenon lamp with a cut-off filter (λ > 420 nm) as the light

source. High purity CO_2 gas (99.9%) was passed through water and then allowed to enter into the reaction setup for reaching ambient pressure. The photocatalyst was allowed to equilibrate in the CO_2/H_2O system for 20 min and then irradiated with visible light. The gaseous products were analyzed online using a gas chromatograph equipped with both TCD and FID detectors (GC-7920, Au Light, Beijing).

Results and discussion

Effects of coupling TP on PDI

The synthesis route of a T-TP/PDI heterojunction is presented in Scheme 1. The PDI nanosheets were first synthesized by a self-assembly procedure in H_2SO_4 solution,[17] and TCPP was introduced to couple with PDI by π–π interactions. Finally, the small TiO_2 nanoparticles obtained by a solvothermal method with $Ti(Obu)_4$ as a raw material were further loaded on the as-fabricated TP/TPI by a controllable assembly process, and denoted as T-TP/PDI. DRS spectra reveal the wide light-absorption nature of PDI, and the optical absorption of PDI did not change significantly after introducing TCPP (Fig. S1a†). The structural features and crystalline phases of PDI and *x*TP/PDI (*x* = 5, 10, and 15) heterojunctions were studied using XRD patterns, as shown in Fig. S1b.† It can be seen that the XRD peaks corresponding to the typical π–π stacking distance between the PDI perylene skeletons with a *d*-spacing of 3.2–3.7 Å can been clearly obtained on PDI.[35] The introduction of TCPP barely influenced the crystal structure of PDI, and the characteristic diffraction peaks detected on TP/PDI heterojunctions are assigned to PDI, mainly due to the tiny loadings of TP. In particular, the peak with a *d*-spacing of 3.57 Å ranging from 24 to 26°, which corresponds to the π–π stacking interaction between PDI molecules adopting twisted arrangements, is enlarged in Fig. 1a. One can see that the characteristic diffraction peak of PDI has an obvious shift after coupling with TP, indicating strengthened π-stacking interactions inside the heterojunction.[36]

Raman spectra were recorded to study the interactions between TP and PDI (Fig. 1b and Fig. S2†). The G bands of PDI exhibit a positive shift (from 1302 cm^{-1} to 1306 cm^{-1} and 1375 cm^{-1} to 1379 cm^{-1}) after loading with TP, verifying the π–π interaction between PDI and TP.[37] Furthermore, FT-IR spectra were recorded to identify the chemical structure and

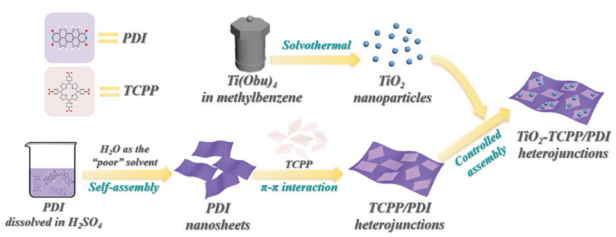

Scheme 1 Schematic illustration of the fabrication of TiO_2-TCPP/PDI (T-TP/PDI) heterojunctions.

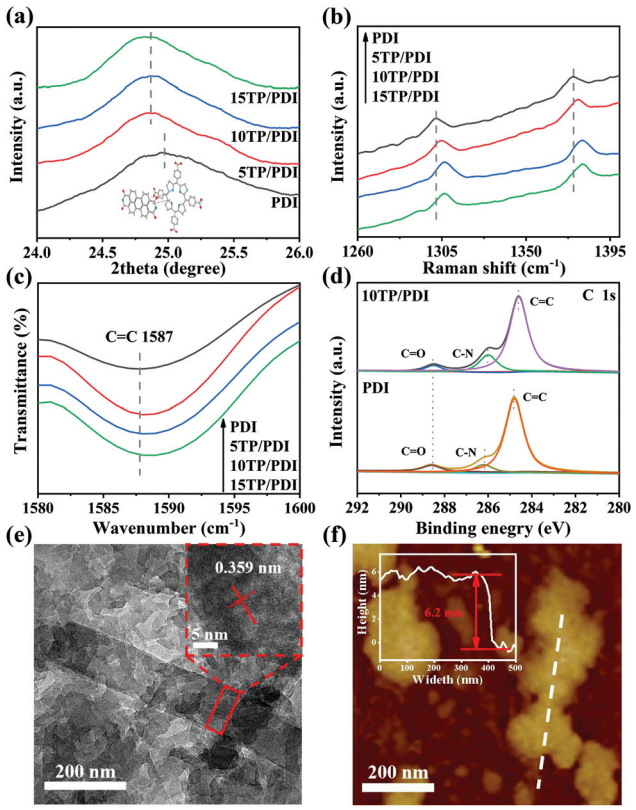

Fig. 1 (a) The partially enlarged view of XRD patterns at 24–26°, (b) Raman spectra with an excitation wavelength of 532 nm, (c) FT-IR spectra of PDI and *x*TP/PDI heterojunctions (*x* represents the mass percentage of TP to PDI), (d) XPS spectra of C 1s for PDI and 10TP/PDI, (e) TEM image of 10TP/PDI with an HRTEM image as the inset, and (f) AFM image and the corresponding height profile of 10TP/PDI.

functional groups of the as-fabricated photocatalysts. As shown in Fig. S3a,† PDI and TP coupled ones show similar FT-IR spectra. Strong absorption bands in the range of 1590–1700 cm^{-1} are associated with the asymmetric/symmetric stretching vibration of the perylene nucleus, whilst the peaks at 744 cm^{-1} and 1349 cm^{-1} correspond to the –N=C=O flexural vibration/stretch and C–N stretch, respectively.[17] It is difficult to distinguish the typical peaks belonging to TP at TP/PDI heterojunctions, which is mainly due to the similar π-electron conjugated organic supramolecular structures of PDI and TP.[38] From the enlarged views of FT-IR spectra as shown in Fig. S3b and S3c,† it can be figured out that the stretching vibration peaks of C=O (1686 cm^{-1}) and C–N (3153 cm^{-1}) detected on PDI remain consistent with those of TP coupled ones, eliminating the H-bond linked interfacial connections. However, the C=C stretching vibration (1587 cm^{-1}) shifts to the direction of high wavenumber with the introduction of TP (Fig. 1c), implying a π–π conjugation dominated interfacial interaction between PDI and TP. This is consistent with the results obtained from XRD and Raman spectra. Moreover, the interfacial relationship between PDI and TP was further revealed by XPS spectra. As shown in

Fig. 1d, the fitted peaks located at around 284.8 eV, 286.1 eV and 288.6 eV are assigned to C=C, C–N and C=O, respectively.[39] As expected, the peak associated with C=C of 10TP/PDI moves to lower binding energy, while the binding energies of C–N, and C=O remain the same. The results of XPS spectra further confirm the π–π interactions between PDI and TP.

The morphology of the 10TP/PDI heterojunction was characterized by transmission electron microscopy (TEM). As shown in Fig. 1e, PDI presents a slender sheet-like structure with a width of *ca.* 100 nm, and its surface is tightly attached by TP. The high-resolution TEM (HRTEM) image shows clear lattice fringes with a characteristic *d*-spacing of 0.359 nm, which matches well with the typical co-facial π–π stacking distance of PDI. Fig. 1f and Fig. S4† show the atomic force microscopy (AFM) images and the corresponding height profiles of pristine PDI and 10TP/PDI heterojunctions. The average thicknesseses of PDI and 10TP/PDI heterojunctions are determined to be 4.9 nm and 6.2 nm, respectively. The increase in the thickness further reveals the face-to-face combination of TP and PDI with the π–π superimposition effect. More specifically, it can be deduced that TP nanosheets are more easily superimposed on PDI due to the similar conjugated structures.

Steady-state surface photovoltage spectroscopy (SS-SPS) is an advanced photophysical technique, which could reveal the photogenerated charge separation and recombination by means of the surface potential difference of a semiconductor before and after illumination.[40] In general, the SPS response has a positive correlation with charge separation. It can be seen from Fig. 2a that all the TP-modified PDI samples show stronger SPS responses than pristine PDI, indicating that the introduction of TP could greatly enhance the charge separation. It is noticed that the SPS response strengthened with the increase of TP loadings, while a decreased signal is observed on the 15TP/PDI nanocomposite with excessive loading amounts. This might be related to the aggregation of TP, which would hinder the charge transfer and separation to some extent. Photoluminescence (PL) spectroscopy was further performed to investigate the charge separation of PDI and a series of *x*TP/PDI nanocomposites (Fig. S5†). Pristine PDI shows the strongest PL signal, indicating severe charge recombination, while the PL signal of PDI quenched after TP coupling, indicating that the charge recombination has been effectively inhibited on *x*TP/PDI ones, in which 10TP/PDI presents the best charge separation properties. The linear sweep voltammetry curves of PDI and *x*TP/PDI heterojunctions were obtained under visible light irradiation (Fig. 2b). It can be seen that the photocurrent densities of *x*TP/PDI heterojunctions are larger than that of PDI, especially the 10TP/PDI one, revealing that TP coupling greatly enhances the charge separation, which is consistent with the results obtained from photophysical measurements. The decreased radius of the semicircle over *x*TP/PDI heterojunctions recorded by electrochemical impedance spectroscopy (EIS) further supports the results of photoelectrochemical measurements (Fig. S6†).

The photocatalytic performance of CO_2 reduction for PDI and *x*TP/PDI heterojunctions was evaluated under visible-light irradiation. Carbon monoxide and methane were detected as the main reduction products. As shown in Fig. 2c, the photoactivity shows a sequential increase with the order of PDI, 5TP/PDI, 15TP/PDI and 10TP/PDI, consistent with the trend of charge transfer and separation properties. In particular, the optimal 10TP/PDI shows 4 times higher photocatalytic activity than pristine PDI. Furthermore, 10TP/PDI was taken as a representative to evaluate the stability during the photocatalytic reactions, and it is found that there is no obvious decay in activity with five consecutive runs of photocatalytic CO_2 reduction, indicative of good stability (Fig. 2d).

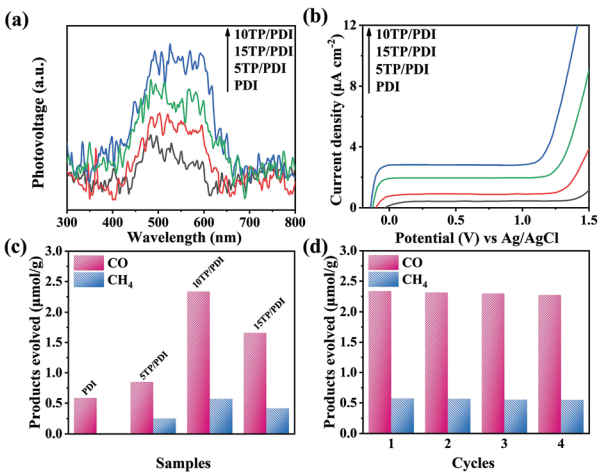

Fig. 2 (a) SPS responses, (b) photoelectrochemical *I*–*V* curves, (c) photocatalytic activities for CO_2 reduction of PDI and *x*TP/PDI heterojunctions under visible-light irradiation and (d) photocatalytic cycling test of the 10TP/PDI heterojunction.

Effects of TiO_2 energy platform on TP/PDI heterojunctions

The energy platform TiO_2 was further introduced and the effects on the as-fabricated *x*TP/PDI heterojunctions were investigated. The obtained TiO_2 is indexed to anatase as evidenced by XRD,[41] while no detectable diffraction peaks assigned to TiO_2 could be recorded on *y*T-10TP/PDI heterojunctions, which might be related to its tiny loading amounts and the high dispersibility (Fig. S7†). Likewise, there is no visible change in the optical absorption of TP/PDI heterojunctions after introducing TiO_2 (Fig. S8†). The morphology and thickness of the representative 5T-TP/PDI were further characterized by TEM and AFM. It can be seen from Fig. 3a that the TiO_2 nanoparticles with a diameter of *ca.* 10 nm are uniformly adhered on the surface of TP (the morphology of pristine TiO_2 is shown in Fig. S9†), and the characteristic *d*-spacing of about 0.35 nm (inset of Fig. 3a) matches well with the (101) planes of TiO_2.[42] Such a microstructure is highly favorable for the interfacial charge transfer from TP to TiO_2. The AFM image and the corresponding height profile show that the average thickness of 5T-10TP/PDI is approximately 6.3 nm (Fig. S10†), which is similar to the 10TP/PDI one.

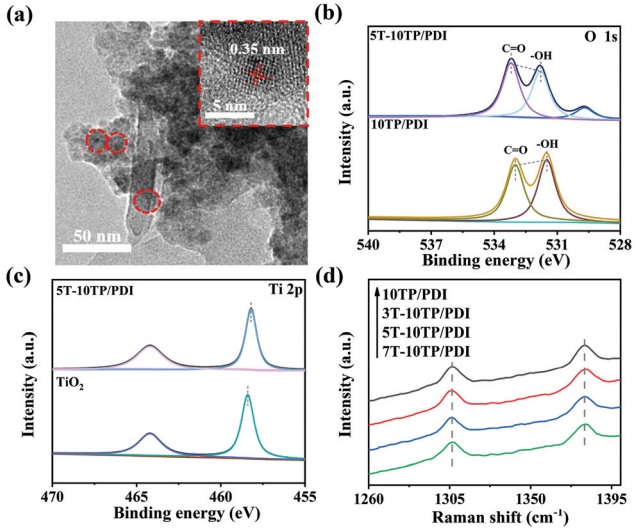

Fig. 3 (a) TEM image of 5T-10TP/PDI with an HRTEM image as the inset, (b) XPS spectra of O 1s for 10TP/PDI and 5T-10TP/PDI, (c) XPS spectra of Ti 2p for TiO_2 and 5T-10TP/PDI, and (d) Raman spectra of 10TP/PDI and *y*T-10TP/PDI heterojunctions (*y* represents the mass percentage of T to PDI).

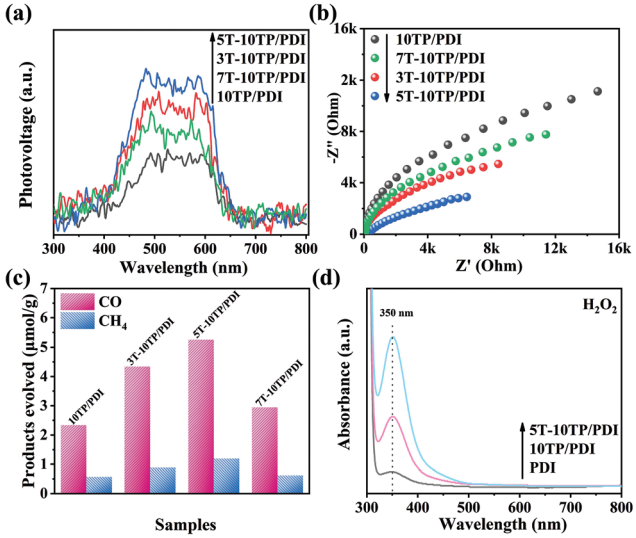

Fig. 4 (a) SPS responses, (b) EIS spectra, (c) photoactivities for CO_2 conversion under visible-light irradiation of 10TP/PDI and *y*T-10TP/PDI heterojunctions, and (d) UV-vis absorption spectra related to the H_2O_2 generation of PDI, 10TP/PDI and 5T-10TP/PDI.

The surface hydroxyl groups are clearly detected on TiO_2 using the FT-IR spectrum (Fig. S11†), which provides great opportunities for the subsequent intimate bonding with TP/PDI heterojunctions. XPS spectra were employed to explore the chemical environment change after coupling with TiO_2. Fig. 3b shows the O 1s spectra of 10TP/PDI and TiO_2 coupled one. The peak located at 529.8 eV associated with lattice oxygen is detected on the 5T-10TP/PDI heterojunction,[43] indicative of the successful introduction of TiO_2. Interestingly, it is noticed that the relative intensity of the fitted hydroxyl oxygen is decreased, which ought to be strengthened due to the additional hydroxyl groups inherited from TiO_2, indicating the effective chemical connection with 10TP/PDI through the hydroxyl groups. Turning to the Ti 2p XPS spectra of the 5T-10TP/PDI heterojunction (Fig. 3c), the binding energies of Ti 2p 3/2 and Ti 2p 1/2 show a negative shift compared with that of bare TiO_2. Based on the above analysis, it can be speculated that an intimate interface is formed through dehydration condensation between the hydroxyl groups of TiO_2 and the carboxyl group of TP. Raman spectra further revealed that the introduced TiO_2 did not affect the π–π interaction between TP and PDI due to the invisible Raman shift on T-10TP/PDI heterojunctions (Fig. 3d and Fig. S12†).

As shown in Fig. 4a, the SPS responses of T-10TP/PDI heterojunctions with different TiO_2 loadings are stronger than that of the 10TP/PDI one, indicating that the introduction of TiO_2 could further enhance the charge separation. 5T-10TP/PDI shows the strongest SPS response, indicating the best charge separation. Fig. S13a† shows the PL spectra of 10TP/PDI and a series of T-10TP/PDI. It can be seen that the PL intensities of T-10TP/PDI are weaker than that of 10TP/PDI, revealing a mitigation of charge recombination by coupling with TiO_2. The linear sweep voltammetry curve of the investigated samples is shown in Fig. S13b.† One can see that the photocurrent densities recorded on TiO_2 coupled ones are much larger than those of 10TP/PDI under visible-light irradiation, especially the 5T-10TP/PDI one. It can be concluded that the introduction of an appropriate amount of TiO_2 could further enhance the charge transfer and separation of the TP/PDI heterojunction. In addition, EIS shows the decreasing impedance radius of T-10TP/PDI heterojunctions (Fig. 4b), evidencing that the interfacial charge transfer resistance of the as-fabricated heterojunction is greatly reduced owing to the presence of TiO_2. Apparently, the results of photoelectrochemical measurements are consistent with photophysical ones.

The performance of photocatalytic CO_2 reduction for 10TP/PDI and those coupled with TiO_2 was evaluated under visible light. As shown in Fig. 4c, the T-10TP/PDI heterojunctions exhibit enhanced activities toward the production of CO and CH_4, and the optimal 5T-10TP/PDI shows a *ca.* 10-times increase in CO production over pristine PDI. Additionally, 5T-10TP/PDI retains the excellent photostability during the process of CO_2 reduction (Fig. S14†). Moreover, the possible oxidation products obtained during CO_2 photoreduction have also been analyzed (Fig. S15†). As expected, a certain amount of O_2 is detected in the investigated samples.

Besides, the photocatalytic CO_2 reduction of 5T-10TP/PDI was also conducted under identical conditions except substituting CO_2 with N_2, and there was no detectable product obtained, demonstrating that the reduction products indeed originate from the conversion of CO_2. It is well recognized that PDI is not favorable for producing hydroxyl radicals,[44] even if the inherent VB is quite deep. Interestingly, H_2O_2 has been found as the intermediate oxidation product by iodimetry with UV-vis characteristic absorption at 350 nm, and the H_2O_2 pro-

duction is gradually increased with the sequence of PDI, 10TP/PDI and 5T-10TP/PDI heterojunctions (Fig. 4d), which is consistent with the results of O_2 evolution. Thus, it is understandable for a transformation pathway from H_2O_2 to O_2 under irradiation.

Mechanism discussion

The time-resolved surface photovoltage (TR-SPV) response is an effective and advanced technique to study the dynamic behavior of photogenerated charge carriers' transfer and separation.[45] The TR-SPV response includes a fast component mainly resulting from the photogenerated charge separation under a built-in electric field, and a slow one mainly attributed to the charge diffusion process, while for nanosized materials, the contribution of the built-in electric field to the SPV is quite small, or even negligible. Accordingly, the TR-SPV signals of PDI and 10TP/PDI mainly originated from the charge diffusion process. As illustrated in Fig. 5a, bare PDI shows a negative TR-SPV signal, presumably related to the nature of some special species on the surface of PDI capturing holes, so that the photogenerated electrons could preferentially diffuse to the electrode surfaces.[46] Significantly, a much stronger TR-SPV response is detected on 10TP/PDI, manifesting that the introduction of TP is beneficial for charge separation, and hence the prolonged lifetime of charge carriers. Furthermore, electron paramagnetic resonance (EPR) measurements were employed to record the produced active species with 5,5-dimethylpyrroline-*N*-oxide (DMPO) as the spin-trapping agent (Fig. 5b). One can see that a quartet of the DMPO-$\bullet O_2^-$ pattern is recorded on pristine PDI, and the signal is strengthened after coupling with TP. This result unambiguously evidences the Z-scheme charge transfer is dominant between PDI and TP, and eliminates the type II transfer pathway. Since the latter one is usually accompanied by a decrease in the thermodynamic energy potential, sufficient driving force cannot be achieved for the formation of more $\bullet O_2^-$ radicals. The estimated energy band alignments of PDI and TP from Mott–Schottky (MS) curves further support the feasibility of the Z-scheme charge transfer pathway (Fig. S16†). As expected, the DMPO-$\bullet O_2^-$ signal of 5T-10TP/PDI is even stronger than that of the 10TP/PDI one, indicating that TiO_2 could be used as an energy platform to accept the electrons transferred from the adjacent TP, and it further facilitates the Z-scheme charge transfer between PDI and TP.

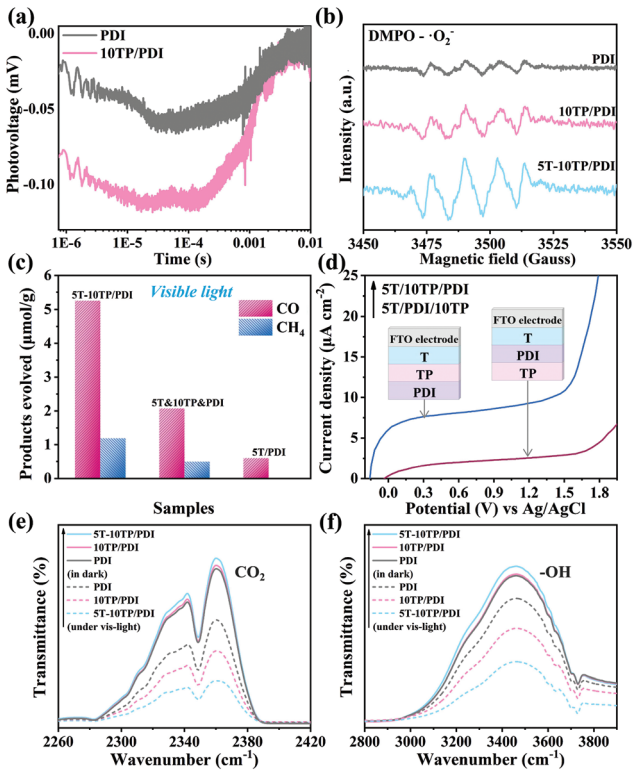

Fig. 5 (a) TR-SPV responses of PDI and 10TP/PDI under a N_2 atmosphere, (b) DMPO spin-trapping EPR spectra recorded for $^{\bullet}O_2^-$ under visible-light irradiation of PDI, 10TP/PDI and 5T-10TP/PDI (detection conditions: the concentration of DMPO was 50 mmol L^{-1}, $^{\bullet}O_2^-$ was determined in methanolic solution), (c) photoactivities of 5T-10TP/PDI, 5T&10TP&PDI and 5T/PDI under visible-light irradiation, and (d) photoelectrochemical *I*–*V* curves of 5T/10TP/PDI and 5T/PDI/10TP with the schematic of the prepared electrodes as the inset. *In situ* DRIFTS spectra of the adsorbed (e) CO_2 and (f) H_2O in the dark for 30 min and then under visible-light irradiation for 30 min of PDI, 10TP/PDI and 5T-10TP/PDI.

To clarify the crucial role of TiO_2 in modulating the Z-scheme transfer and separation and the rational combination of TiO_2 and TP, TiO_2 coupled PDI (T/PDI) and a mechanical mixture of TiO_2, TP and PDI (5T&10TP&PDI) were prepared. It can be found from Fig. 5c that the photocatalytic activity of 5T/PDI is roughly the same as that of PDI, indicating that the coupled TiO_2 has little impact on the activity of PDI. On the other hand, the photocatalytic activity of 5T&10TP&PDI is much lower than that of the rationally designed 5T-10TP/PDI catalyst, disclosing that the intimate interfacial connection between TP and TiO_2 is quite crucial for the directed charge transfer from TP to the energy platform TiO_2. This result is further confirmed by the SPS spectra, that is, 5T-10TP/PDI exhibits a much stronger SPS response than its 5T&10TP&PDI counterpart, corresponding to better charge separation properties (Fig. S17†).

To further verify the role of TiO_2 in the directional Z-scheme charge transfer, TiO_2, TP and PDI with diverse sequences were coated on FTO glass and their photoelectrochemical properties were investigated. In a controlled experiment, TiO_2 was placed on top of PDI (5T/PDI/10TP) instead of TP (5T/10TP/PDI) and their photocurrent densities were measured (Fig. 5d). It can be seen that the photocurrent density of 5T/10TP/PDI is much higher than that of 5T/PDI/10TP under visible-light irradiation, implying that the Z-scheme charge separation could be enhanced only if TiO_2 closely attached on TP. The above-mentioned results clearly evidence that TiO_2 plays a crucial role in manipulating the Z-scheme charge transfer on the well-designed 5T-10TP/PDI heterojunction.

In view of the fact that –COOH groups in TP play a crucial role in the intimate connection between TP and TiO_2, and

further cascade Z-scheme charge separation, PDI coupled tetraphenylporphyrin (TPP) without carboxyl group grafting was fabricated and denoted as TPP/PDI. As shown in Fig. S18,† albeit the photoactivity of pristine PDI could be improved after TPP coupling, the photocatalytic activity of 10TPP/PDI is far from that of the 10TP/PDI heterojunction, let alone the 5T-10TP/PDI one. Even if TiO_2 is further modified on 10TPP/PDI, the difference of photoactivities between 5T-10TPP/PDI and 10TPP/PDI is quite small, implying that –COOH groups have a considerable effect on the photocatalytic activities. As disclosed by FT-IR spectra (Fig. S19†), the C=C characteristic stretching vibration peak of PDI shifts to 1587 cm^{-1} with TPP introduction, indicative of a strong π–π interaction between TPP and PDI. Raman spectra further support the above results (Fig. S20†), while the binding energy of Ti 2p for 5T-10TPP/PDI is roughly the same as that of bare TiO_2, indicating that the connection between TPP and TiO_2 is rather weak (Fig. S21†). All these results confirm the importance of carboxyl groups in TP.

To disclose the change of the adsorbed reaction molecules on the surfaces of photocatalysts during the photocatalytic CO_2 reduction process, *in situ* diffuse reflectance infrared Fourier transform spectroscopy (DRIFTS) was performed in the condition of CO_2 (g) carrying H_2O (Fig. 5e and h). The absorption peaks in the region from 2200 to 2400 cm^{-1} are assigned to the asymmetric stretching vibration of the CO_2 molecule,[47] and the adsorption peaks for the surface –OH stretching of H_2O are observed in the range of 3500–3800 cm^{-1}.[48] It can be seen that the –OH stretching peaks of PDI and 10TP/PDI are similar, while they are much stronger on the 5T-10TP/PDI photocatalyst, indicating that the coupled small TiO_2 particles are favorable for water adsorption. Turning to the condition of CO_2 adsorption, it can be seen that a barely visible difference could be observed on PDI, 10TP/PDI and TiO_2 coupled one. It is noteworthy that under visible-light irradiation, one can see that the H_2O adsorption bands of PDI and 10TP/PDI are weakened in sequence, and it is much obvious on 5T-10TP/PDI. The CO_2 conversion process is consistent with that of H_2O. This implies that the accelerated process of CO_2 conversion is mainly ascribed to the strengthened Z-scheme charge transfer along with the favorable adsorption and activation of H_2O molecules on account of the small sized TiO_2 introduction.

Accordingly, a schematic diagram of photocatalytic CO_2 reduction along with the involved charge transfer and separation by the well-designed 5T-10TP/PDI is presented in Scheme 2. Electron–hole pairs are generated in both PDI and TP under visible-light excitation. The photo-induced electrons on the CB of PDI would transfer to the HOMO of TP following the Z-scheme pathway, and the spatially separated electrons of TP could be further transferred to the surface of the energy platform TiO_2 where CO_2 reduction to CO and CH_4 occurs, while photoholes are left on the VB of PDI to oxidize H_2O to the intermediate H_2O_2, and further the O_2.

Moreover, the wide band gap oxide SnO_2 was employed to substitute TiO_2 and the influence on the 10TP/PDI heterojunction was investigated. The XRD pattern in Fig. S22† shows the successful synthesis of SnO_2. It can be found that both the photoactivity and charge separation of 10TP/PDI could be further improved after introducing SnO_2 (Fig. S23†). This further proves that the built energy platform strategy for modulating the Z-scheme charge transfer is applicable for other wide bandgap semiconductors with appropriate CB levels.

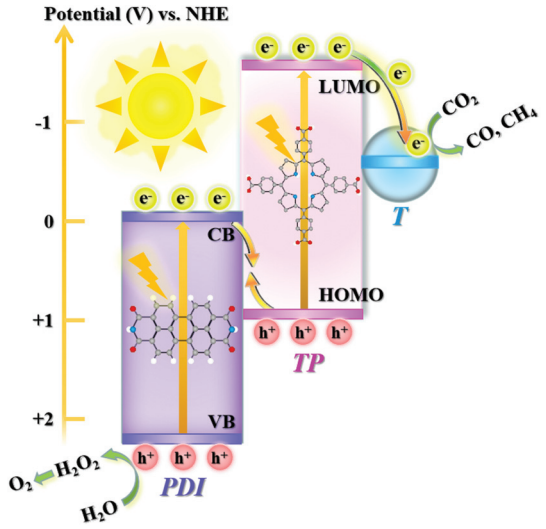

Scheme 2 Schematic of the proposed Z-scheme charge transfer process along with the induced redox reactions on T-TP/PDI heterojunctions. TP and T refer to TCPP and TiO_2, respectively.

Conclusions

To summarize, a full-spectrum responsive Z-scheme nano-heterojunction of T-TP/PDI has been fabricated for efficient CO_2 reduction. The optimal one delivers an ~10-time enhancement in photocatalytic activity compared with pristine PDI. The improved activity mainly lies in the promoted Z-scheme charge transfer with robust interfacial interactions between PDI and TP, along with the directed charge transfer by the introduced energy platform TiO_2. The coupled TiO_2 could effectively extract the photoelectrons accumulated on the CB of TP so as to strengthen the Z-scheme charge transfer and hence to inhibit the undesirable type-II charge transfer between TP and PDI. This work provides a feasible route to construct efficient PDI-based Z-scheme nano-heterojunction photocatalysts for solar-driven CO_2 reduction.

Author contributions

Yilin Wang: data curation and writing–original draft. Zhenlong Zhao: data curation and investigation. Rui Sun: methodology. Ji Bian: writing – review and editing. Ziqing Zhang: conceptualization and writing – review and editing. Liqiang Jing: conceptualization, methodology, supervision, writing – review and editing, project administration, and funding acquisition. All

authors have given approval for the final version of the manuscript.

Conflicts of interest

There are no conflicts to declare.

Acknowledgements

This work was financially supported by the National Natural Science Foundation of China (U1805255, U2102211, and 22105066).

References

1 Y. Liang, L. Polvani and I. Mitevski, *Science*, 2022, **5**, 1.
2 L. Dong, L. Zhang, J. Liu, Q. Huang, M. Lu, W. Ji and Y. Lan, *Angew. Chem., Int. Ed.*, 2020, **59**, 2659.
3 J. Katrina and F. Moore, *Nature*, 2021, **598**, 262.
4 T. Ju, Y. Zhou, K. Cao, Q. Fu, J. Ye, G. Sun, X. Liu, L. Chen, L. Liao and D. Yu, *Nat. Catal.*, 2021, **4**, 304.
5 Y. Ma, X. Yi, S. Wang, T. Li, B. Tan, C. Chen, T. Majima, E. Waclawik, H. Zhu and J. Wang, *Nat. Commun.*, 2022, **13**, 1400.
6 X. Jiao, K. Zheng, L. Liang, X. Li, Y. Sun and Y. Xie, *Chem. Soc. Rev.*, 2020, **49**, 6592.
7 Z. Wang, Q. Wan, Y. Shi, H. Wang, Y. Kang, S. Zhu, S. Lin and L. Wu, *Appl. Catal., B*, 2021, **288**, 120000.
8 X. Zhu, Z. Wang, K. Zhong, Q. Li, P. Ding, Z. Feng, J. Yang, Y. Du, Y. Song, Y. Hua, J. Yuan, Y. She, H. Li and H. Xu, *Chem. Eng. J.*, 2022, **419**, 132204.
9 Y. Shi, J. Li, C. Mao, S. Liu, X. Wang, X. Liu, S. Zhao, X. Liu, Y. Huang and L. Zhang, *Nat. Commun.*, 2021, **12**, 5923.
10 X. Chen, J. Wang, Y. Chai, Z. Zhang and Y. Zhu, *Adv. Mater.*, 2021, **33**, 2007479.
11 X. Feng, Y. An, Z. Yao, C. Li and G. Shi, *ACS Appl. Mater. Interfaces*, 2012, **4**, 614.
12 L. Zong, Y. Gong, Y. Yu, Y. Xie, G. Xie, Q. Peng, Q. Li and Z. Li, *Sci. Bull.*, 2018, **63**, 108.
13 R. Siram, M. Khenkin, A. Niazov-Elkan, K. Anoop, H. Weissman, E. Katz, I. Visoly-Fisher and B. Rybtchinski, *Nanoscale*, 2019, **11**, 3733.
14 F. Pan, C. Sun, Y. Li, D. Tang, Y. Zou, X. Li, S. Bai, X. Wei, M. Lv, X. Chen and L. Li, *Energy Environ. Sci.*, 2019, **12**, 3400.
15 P. Scheurle, A. Biewald, A. Mähringer, A. Hartschuh, D. Medina and T. Bein, *Small Struct.*, 2022, 2100195.
16 L. Zeng, T. Liu, C. He, D. Y. Shi, F. Zhang and C. Duan, *J. Am. Chem. Soc.*, 2016, **138**, 3958.
17 D. Liu, J. Wang, X. Bai, R. Zong and Y. Zhu, *Adv. Mater.*, 2016, **28**, 7284.
18 W. Zhang, A. Mohamed and W. Ong, *Angew. Chem., Int. Ed.*, 2020, **59**, 22894.
19 J. Low, B. Dai, T. Tong, C. Jiang and J. Yu, *Adv. Mater.*, 2019, **31**, 1802981.
20 Y. Qi, Y. Zhao, Y. Gao, D. Li, Z. Li, F. Zhang and C. Li, *Joule*, 2018, **2**, 2393.
21 H. Gong, Y. Zhang, Y. Cao, M. Luo, Z. Feng, W. Yang, K. Liu, H. Cao and H. Yan, *Appl. Catal., B*, 2018, **237**, 309.
22 Z. Jiang, W. Wan, H. Li, S. Yuan, H. Zhao and P. Wong, *Adv. Mater.*, 2018, **30**, 170618.
23 T. Cai, W. Zeng, Y. Liu, L. Wang, W. Dong, H. Chen and X. Xia, *Appl. Catal., B*, 2020, **263**, 118327.
24 P. Xia, B. Zhu, B. Cheng, J. Yu and J. Xu, *ACS Sustainable Chem. Eng.*, 2018, **6**, 965–973.
25 W. Wang, G. Chen, C. Li, Z. Han, Y. Hu and Q. Meng, *Nanoscale*, 2018, **10**, 5239.
26 Y. Ma, Y. Bian, Y. Liu, A. Zhu, H. Wu, H. Cui, D. Chu and J. Pan, *ACS Sustainable Chem. Eng.*, 2018, **6**, 2552.
27 X. Hao, Y. Wang, J. Zhou, Z. Cui, Y. Wang and Z. Zou, *Appl. Catal., B*, 2018, **221**, 302.
28 Z. Zhang, Y. Zhu, X. Chen, H. Zhang and J. Wang, *Adv. Mater.*, 2019, **31**, 1806626.
29 W. Dai, L. Jiang, J. Wang, Y. Pu, Y. Zhu, Y. Wang and B. Xiao, *Chem. Eng. J.*, 2020, **397**, 125476.
30 R. Ikreedeegh and M. Tahir, *J. Environ. Chem. Eng.*, 2021, **9**, 105600.
31 J. Bian, Z. Zhang, J. Feng, M. Thangamuthu, F. Yang, L. Sun, Z. Li, Y. Qu, D. Tang, Z. Lin, F. Bai, J. Tang and L. Jing, *Angew. Chem., Int. Ed.*, 2021, **60**, 2.
32 H. Hussain, G. Tocci, T. Woolcot, X. Torrelles, C. Pang, D. Humphrey, C. Yim, D. Grinter, G. Cabailh, O. Bikondoa, R. Lindsay, J. Zegenhagen, A. Michaelides and G. Thornton, *Nat. Mater.*, 2017, **16**, 461.
33 H. Gao, J. Wang, M. Jia, F. Yang, R. Andriamitantsoa, X. Huang, W. Dong and G. Wang, *Chem. Eng. J.*, 2019, **374**, 684.
34 C. Zhang, P. Chen, H. Dong, Y. Zhen, M. Liu and W. Hu, *Adv. Mater.*, 2015, **27**, 5379.
35 R. Sun, H. Yin, Z. Zhang, Y. Wang, T. Lang, S. Zhang and L. Jing, *J. Phys. Chem. C*, 2021, **125**, 23830.
36 J. Yang, H. Miao, Y. Wei, W. Li and Y. Zhu, *Appl. Catal., B*, 2019, **240**, 225.
37 Y. Wei, M. Ma, W. Li, J. Yang, H. Miao, Z. Zhang and Y. Zhu, *Appl. Catal., B*, 2018, **238**, 302.
38 Y. Chen, C. Yan, J. Dong, W. Zhou, F. Rosei, Y. Feng and L. Wang, *Adv. Funct. Mater.*, 2021, **31**, 2104099.
39 Y. Sheng, H. Miao, J. Jing, W. Yao and Y. Zhu, *Appl. Catal., B*, 2020, **272**, 118897.
40 X. Li, Q. Zhang, B. Li, Z. Li, Z. Zhang and L. Jing, *Chem. Res. Chin. Univ.*, 2021, **36**, 1116.
41 J. Pan, Z. Dong, B. Wang, Z. Jiang, C. Zhao, J. Wang, C. Song, Y. Zheng and C. Li, *Appl. Catal., B*, 2019, **242**, 92.
42 Y. Wu, F. Gao, H. Wang, L. Kovarik, B. Sudduth and Y. Wang, *J. Phys. Chem. C*, 2021, **125**, 3988.
43 F. Xu, L. Zhang, B. Cheng and J. Yu, *ACS Sustainable Chem. Eng.*, 2018, **6**, 12291.
44 Q. Gao, J. Xu, Z. Wang and Y. Zhu, *Appl. Catal., B*, 2020, **271**, 118933.

45 L. Zhang, S. Li, B. Liu, D. Wang and T. Xie, *ACS Catal.*, 2014, **4**, 3724.
46 R. Sun, Y. Wang, Z. Zhang, Y. Qu, Z. Li, B. Li, H. Wu, X. Hua, S. Zhang, F. Zhang and L. Jing, *Chem. Eng. J.*, 2021, **426**, 131266.
47 Y. Liu, Y. Li, X. Li, Q. Zhang, H. Yu, X. Peng and F. Peng, *ACS Nano*, 2020, **14**, 14181.
48 P. Yang, R. Wang, H. Tao, Y. Zhang, M. Titirici and X. Wang, *Appl. Catal., B*, 2021, **280**, 119454.